Chem. Eng. Comm., 192: 89–107, 2005

ISSN: 0098-6445 print/1563-5201 online
DOI: 10.1080/00986440590473263

Taylor & Francis
Taylor & Francis Group

Shear Thickening in Dilute Polymer Solutions: Transient Analysis

P. A. KAMERKAR
B. J. EDWARDS
D. J. KEFFER
C. W. RENEAU

Department of Chemical Engineering,
The University of Tennessee,
Knoxville, Tennessee

Transient shear properties of dilute polymer solutions are investigated in the shear rate regions where shear thickening can occur. Comparison of transient rheological and optical data with the two coupled Maxwell modes model offers insight into the physical mechanisms that give rise to this anomalous behavior. Specifically, shear thickening occurs due to the deterioration of the size and anisotropy of structures deformed at lower shear rates. Coincident theoretical and experimental discontinuities in the transient profiles of the dichroic orientation angle appear to confirm the prior statement.

Keywords: Shear thickening; Dilute polymer solutions; Birefringence; Dichroism

Introduction

It is well known that dilute polymeric solutions typically display *shear-thinning* behavior under the application of shear; i.e., their viscosities decrease with increasing shear rate (Bird et al., 1987). However, some of these fluids exhibit an anomalous behavior at high shear rates: it has been observed that, under very specific conditions, their viscosities actually increase with the magnitude of applied shear rate, provided the rate of shear is large enough (Kishbaugh, 1992; Kishbaugh and McHugh, 1993; Layec-Raphalen and Wolff, 1976; Vrahopoulou and McHugh 1987). This phenomenon is called *shear thickening*. One of the manifestations of shear thickening can occur in dilute, low-viscosity solutions when the molecular weight of the dissolved polymer is very high, the concentration of polymer lies within a certain range, and the shear rate is relatively large.

Ten years ago, the cause of shear thickening in these dilute solutions was finally resolved. The work by Kishbaugh and McHugh (Kishbaugh, 1992; Kishbaugh and McHugh, 1993a,b) provided the definitive connection between the anomaly of shear thickening at high shear rates and shear-induced structure formation. They found

Received 22 July 2002; in final form 26 May 2003.
Address correspondence to B. J. Edwards, Department of Chemical Engineering, University of Tennessee, 429 Dougherty Engineering Building, Knoxville, TN 37917.

that shear thickening arises due to *intermolecular* interactions, not *intramolecular* interactions, as ascertained through extensive experimentation: a rheo-optical technique was used to measure the rheological and optical responses of the solutions in the initial shear-thinning regime and subsequent shear-thickening region. The results of the experiments conclusively demonstrated that the shear-thickening behavior was associated with supermolecular structure formation.

Although the experimental investigations of Kishbaugh and McHugh could delineate the phenomenon of shear thickening in polymeric solutions, there was no self-consistent theory that could potentially describe all of the experimental observations at that time. However, the recent work by Edwards et al. (2002) provided a single theory that could explain both the rheological and optical behavior simultaneously, while offering predictions for rheological characteristic functions, such as the first and second normal stress coefficients, that were not measured experimentally.

According to the two coupled Maxwell modes (TCMM) model (Edwards et al., 2002), associations (or structures) of the individual polymer chains start growing in size and aspect ratio at small values of the shear rate below $\dot{\gamma}_c$, the critical shear rate for the onset of shear thickening (see Figure 1). These associations actually lower the viscosity in the solution by relieving some of the stress acting on the polymer chains as the structures increase in size and aspect ratio. This augments the natural intramolecular chain shear thinning of the dilute solutions. At the critical shear rate, $\dot{\gamma}_c$, these structures become too distended to be supported by the hydrodynamic forces acting on them. This results from the decrease in viscosity of the shear-thinning solution. Thus the structures begin to decrease in size and aspect ratio in response to the lowered degree of shear force exerted upon them. This reduction in size restricts the stress relief offered to the solution dynamics, and, consequently, the viscosity increases with increasing shear rate. At higher values of the shear rate, the structures become totally isotropic, at $\dot{\gamma}_m$, at which point a shear-thinning

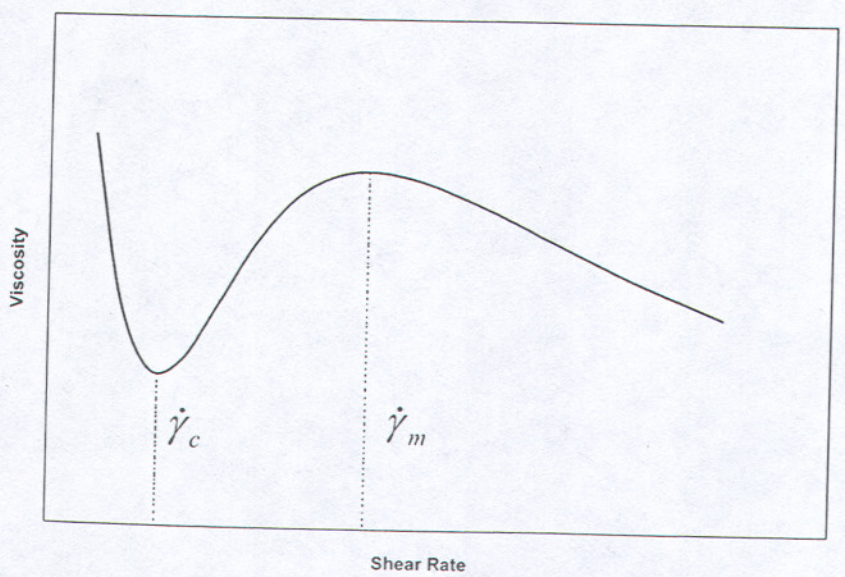

Figure 1. Generic profile of viscosity versus shear rate for a dilute polymer solution that exhibits shear thickening.

behavior resumes as the intra-chain dynamics again dictate the qualitative behavior of the shear viscosity curve (see Figure 1).

In the previous publication (Edwards et al., 2002), the analysis was limited to steady-state shear flow; however, the rheological and optical experimental data of Kishbaugh and McHugh (Kishbaugh, 1992; Kishbaugh and McHugh,1993a) also contained limited transient data taken during start-up, steady state, and cessation of the shear flow experiments. This transient behavior is very interesting in its own right and can also be described by the TCMM model. Indeed, as we shall see, it can also be used to add further credibility to the predictions of said model. Consequently, in this article, we extend the analysis of Edwards et al. (2002) from the steady flow regime to the transient flow regime and compare predictions of the TCMM model with the transient flow experiments of Kishbaugh and McHugh (Kishbaugh, 1992; Kishbaugh and McHugh, 1993a). Also, as in the preceding article, we offer predictions for rheological properties (but time-dependent predictions this time) that have not been measured experimentally.

The Two Coupled Maxwell Modes Model

The TCMM model characterizes the essential qualitative and semi-quantitative behavior of polymeric fluids (Edwards et al., 1996). It has evolved from the thermodynamic methodology developed by Grmela (1988, 1989) and Beris and Edwards (Beris and Edwards, 1994; Edwards and Beris, 1991a,b).The multiple coupled Maxwell modes model was first introduced in Beris and Edwards (1994) and reduced to a two-mode version in Edwards et al. (1996). Use of this two-mode model was shown to reproduce faithfully (Edwards et al., 1996) all of the essential qualitative features of polymeric viscoelastic fluids; quantitative reproductions can be achieved through the use of additional (often uncoupled) modes.

To examine the behavior of dilute polymer solutions with structure formation, the TCMM model is applied using two second-rank mode-conformation tensors, $\mathbf{c}^1$ and $\mathbf{c}^2$. The first mode-conformation tensor, $\mathbf{c}^1(\mathbf{x}, t)$, is the second moment of the orientational distribution function, $\psi(\mathbf{x}, \mathbf{R}, t)$ (Bird et al., 1987):

$$\mathbf{c}^1 = \int \mathbf{RR}\,\psi\, d^3R \tag{1}$$

In this expression, $\mathbf{R}$ is the end-to-end vector of a dissolved polymer chain and $\mathbf{x}$ is the Eulerian coordinate denoting the spatial position of the chain's center of mass. According to Equation (1), $\mathbf{c}^1$ has units of length squared. The second mode tensor, $\mathbf{c}^2(\mathbf{x}, t)$, quantifies the size, shape, and orientation of the intermolecular structures that are formed during shear (Edwards et al., 2002). Using as the size distribution function $f(\mathbf{x}, \mathbf{a}, t)$, with $\mathbf{a}$ the vector spanning the major axis of a spheroidal structure, the second mode tensor can be defined as (Edwards et al., 2002)

$$\mathbf{c}^2 = \int \mathbf{aa}\, f\, d^3a \tag{2}$$

The eigenvalues and eigenvectors of these second-rank tensors quantify the degree of orientation and the characteristic directions, respectively, of the two relaxation modes (Edwards et al., 1996, 2002).

In a homogeneous flow field, the evolution equations for the mode-conformation tensors can be decoupled from the Cauchy momentum equation and

solved independently for known kinematics. These evolution equations are

$$\frac{\partial c^1_{\alpha\beta}}{\partial t} - c^1_{\alpha\gamma}\nabla_\gamma v_\beta - c^1_{\beta\gamma}\nabla_\gamma v_\alpha = -\frac{1}{\lambda_1}c^1_{\alpha\beta} + \frac{k_B T}{\lambda_1 K_1}\delta_{\alpha\beta} - \frac{\theta}{2k_B T}\sqrt{\frac{n_2}{n_1}}\frac{1}{\sqrt{\lambda_1\lambda_2}} \times \left[K_2\left(c^1_{\alpha\gamma}c^2_{\beta\gamma} + c^2_{\alpha\gamma}c^1_{\beta\gamma}\right) - 2k_B T c^1_{\alpha\beta}\right]$$

$$\frac{\partial c^2_{\alpha\beta}}{\partial t} - c^2_{\alpha\gamma}\nabla_\gamma v_\beta - c^2_{\beta\gamma}\nabla_\gamma v_\alpha = -\frac{1}{\lambda_2}c^2_{\alpha\beta} + \frac{k_B T}{\lambda_2 K_2}\delta_{\alpha\beta} - \frac{\theta}{2k_B T}\sqrt{\frac{n_2}{n_1}}\frac{1}{\sqrt{\lambda_1\lambda_2}} \times \left[K_1\left(c^1_{\alpha\gamma}c^2_{\beta\gamma} + c^2_{\alpha\gamma}c^1_{\beta\gamma}\right) - 2k_B T c^2_{\alpha\beta}\right]$$

In these expressions, k_B is the Boltzmann constant, T is the absolute temperatu K_1, K_2 are the Hookean spring constants of the free polymer chains and structur (respectively), λ_1, λ_2 are the relaxation times of the two modes, n_1, n_2 are the effecti concentrations, and θ is the degree of interaction between the two modes. For t model to be physically feasible, λ_1, λ_2, n_1, and n_2 must all have values greater tha or equal to zero. Thermodynamically, it appears that θ should lie within the ran of $[-1, 1]$. It is typically a small positive fraction (Edwards et al., 1996; Beris an Edwards, 1994).

Rheological Properties

According to the TCMM model (Edwards et al., 1996; Beris and Edwards, 1994), th extra stress tensor is given by a linear sum over the two mode-conformation tensors

$$\sigma_{\alpha\beta} = \sum_{i=1}^{2}\left(n_i N_A K_i c^i_{\alpha\beta} - n_i N_A k_B T\delta_{\alpha\beta}\right) \quad (5$$

where N_A is Avogadro's number. This second-rank tensor has units of force pe length squared, and the shear viscosity, η, is calculated by dividing the shear stres component, σ_{12}, by the shear rate, $\dot{\gamma}$. The first and second normal stress coefficients are defined as $\Psi_1 \equiv (\sigma_{11} - \sigma_{22})/\dot{\gamma}^2$ and $\Psi_2 \equiv (\sigma_{22} - \sigma_{33})/\dot{\gamma}^2$, respectively.

Optical Properties: Dichroism

The TCMM model describes more than just the rheological properties of polymeric materials: it can also be used to determine the optical properties of the deforming liquid. The dichroic signal, $\Delta n''$, is calculated using both modes by summation of the following two equations (Kishbaugh, 1992; Kishbaugh and McHugh, 1993b; Edwards et al., 2002):

$$\Delta n''_1 = \frac{4\pi}{5}k^3\frac{cN_A m_s}{M}(\alpha_1^2 - \alpha_2^2)_1[\mathrm{tr}\,\tilde{\mathbf{c}}^1 - 3] \quad (6)$$

$$\Delta n''_2 = \frac{8\pi}{15}m_p n_2 N_A k_3(\alpha_1^2 - \alpha_2^2)_2\frac{h}{(1 + 36/\sigma^2)} \quad (7)$$

The first equation, Equation (6), is the innate dichroism of the individual polymer chains. The parameters appearing in this equation are: wave number, $k = (2\pi/6.328 \times 10^{-7})\mathrm{m}^{-1}$, polymer concentration, c, molecular weight, M, the refractive

index of the solvent, $m_s = 1.475$ (Kishbaugh, 1992; Kishbaugh and McHugh, 1993b), and the polarizability difference, $(\alpha_1^2 - \alpha_2^2)_1$. This last quantity was estimated by Kishbaugh and McHugh as -1.25×10^{-42} cm^3/molecule using the method of Gurnee (1954). Since $\mathrm{tr}\,\tilde{\mathbf{c}}^1$ is always greater than three, this contribution to the dichroic signal is always negative in sign.

The second equation, Equation (7), is the dichroism arising from the supermolecular structures according to the Rayleigh scattering theory (Kishbaugh, 1992; Kishbaugh and McHugh, 1993b; Edwards et al., 2002). The quantities appearing in this expression are the refractive index of the polymer, $m_p = 1.59$ (Kishbaugh, 1992; Kishbaugh and McHugh, 1993b), and several other model-specific functions. The first is an anisotropy function that depends on the shape of the structure, p:

$$b = \frac{p^2 - 1}{p^2 + 1} \tag{8}$$

with p taken as (Edwards et al., 2002)

$$p = \left(1 + \frac{3}{2}[\mathrm{tr}\tilde{\mathbf{c}}^2 - 3]\right)^{3/4} \tag{9}$$

The quantity σ is a dimensionless measure of the shear rate relative to the size and shape of the assumed structures. It is given by (Kishbaugh, 1992; Kishbaugh and McHugh, 1993b)

$$\sigma = \frac{\eta_S V_P v(p)}{k_B T}\dot{\gamma} \tag{10}$$

where V_p is the volume of the structure,

$$V_P = \frac{4\pi}{3p^2}a^3 = \frac{4\pi}{3p^2}([\mathrm{tr}\,\tilde{\mathbf{c}}^2 - 3]\langle\mathbf{aa}\rangle_0)^{3/2} \tag{11}$$

$\eta_S = 2.79$ cP for decalin, the solvent, at 25°C, and

$$\frac{1}{v(p)} = \frac{p^2}{p^4 + 1}\left(-1 + \frac{2p^2 - 1}{2p\sqrt{p^2 - 1}}\ln\left[\frac{p + \sqrt{p^2 - 1}}{p - \sqrt{p^2 - 1}}\right]\right) \tag{12}$$

In Equation (11), $\langle\mathbf{aa}\rangle_0$ is the diameter squared of the average structure in the limit of vanishing shear rate. A measure of the structure size can be obtained from $a = \sqrt{(\lambda_p - 1)\langle\mathbf{aa}\rangle_0}$, where λ_p is the primary eigenvalue of $\tilde{\mathbf{c}}^2$ (Edwards et al., 2002). The last quantity appearing in Equation (7) is the polarizability difference of the structures, $(\alpha_1^2 - \alpha_2^2)_2$. It is given by (Kishbaugh, 1992; Kishbaugh and McHugh, 1993b; Edwards et al., 2002)

$$\frac{16\pi^2}{V_P^2}(\alpha_1^2 - \alpha_2^2)_2 = \left(\frac{1}{L_1 + 1/(m_s^2 - 1)}\right)^2 - \left(\frac{1}{L_2 + 1/(m_s^2 - 1)}\right)^2 \tag{13}$$

where

$$L_1 = \frac{1 - e^2}{e^2}\left(-1 + \frac{1}{2e}\ln\left[\frac{1 + e}{1 - e}\right]\right) \tag{14}$$

$$L_2 = \frac{1 - L_1}{2}$$

$$e^2 = \left(1 - \frac{1}{p^2}\right)$$

It can be shown that the contribution to the dichroic signal arising from the str tures is always greater than or equal to zero.

It is important to note a hypothesis expressed in the previous study (Edwar et al., 2002): the dichroic orientation angle is dependent on which mode domina the dichroism. When anisotropic structures are present, they dominate the dichr signal since $\Delta n_2''$ is of greater magnitude than $\Delta n_1''$. Thus, for shear rates with signi cant structural anisotropy, the dichroic orientation angle is quantified by t primary eigenvector of $\tilde{\mathbf{c}}^2$. However, for extremely high values of the shear rate, aft the dichroic signal has switched from positive to negative, this signal is no dominated by the free polymer chains, and thus the dichroic orientation angle quantified by the primary eigenvector of $\tilde{\mathbf{c}}^1$. This hypothesis will be confirmed in th article.

Optical Properties: Birefringence

The TCMM model also allows calculation of the linear birefringence, $\Delta n'$, accordin to the following equation (Kishbaugh, 1992; Kishbaugh and McHugh, 1993b Edwards et al., 2002):

$$\Delta n' = 2\pi \frac{n_1 N_A}{\omega} m_s \left([\mathrm{tr}\,\tilde{\mathbf{c}}^1 - 3]\Theta_i + [\mathrm{tr}\,\tilde{\mathbf{c}}^1 - 3]\Theta_{fs} + 4\pi e_1 \Theta_f\right) \tag{17}$$

Three types of birefringence contribute to $\Delta n'$, but all of them arise from the free polymer chains: the birefringence associated with the anisotropy of the supermole cular structures is several orders of magnitude smaller than that calculated accord ing to the above expression (Kishbaugh, 1992; Kishbaugh and McHugh, 1993b; Edwards et al., 2002), and is therefore excluded from Equation (17). The quantity ω appearing in Equation (17) is a magnitude corrector for the birefringence (Edwards et al., 2002). It essentially acts as another fitting parameter in the present study.

The first term in Equation (17) represents the intrinsic optical anisotropy of the free polymer chains. This term is proportional to Θ_i, which is given by (Kuhn and Grün, 1942)

$$\Theta_i = \frac{3}{5}(\alpha_1 - \alpha_2)_1 \tag{18}$$

The polarizability difference, $(\alpha_1 - \alpha_2)_1 = -5.49 \times 10^{-24}\,\mathrm{cm}^3$/molecule, is assigned the value calculated by Kishbaugh and McHugh (Kishbaugh, 1992; Kishbaugh and McHugh, 1993b) using the method of Gurnee (1954). This contribution to the birefringent signal is always negative in sign.

The second contribution to the overall birefringence is of macroform anisotropy (Copic, 1957), which is due to the difference in the refractive indices of the polymer and solvent. In Equation (17), this contribution is given by (Kishbaugh, 1992;

Kishbaugh and McHugh, 1993b; Edwards et al., 2002)

$$\Theta_f = \left(\frac{m_s^2 + 2}{3}\right)^2 \left(\frac{m_p^2 - m_s^2}{4\pi m_s \rho N_A}\right)^2 \frac{M^2}{v} \tag{19}$$

with

$$e_1^2 = \left(1 - \frac{1}{p_1^2}\right) \tag{20}$$

Note that p_1 appearing in Equation (20) is a function of the trace of the first mode-conformation tensor, $p_1 = (1 + \frac{3}{2}[\mathrm{tr}\,\tilde{\mathbf{c}}^1 - 3])^{3/4}$ (Edwards et al., 2002). Furthermore, $\rho = 1.065\,\mathrm{g/mL}$ for polystyrene and $M^2/v = 2.083 \times 10^{25} M^{0.42}$. This contribution to $\Delta n'$ is always positive.

Microform anisotropy (Tsvetkov, 1964) accounts for the third contribution to the birefringence. It increases with the extension of the polymer chain, although it is still an effect arising from the difference in refractive indices between the polymer molecules and solvent. The contribution is expressed by

$$\Theta_{fs} = \frac{3}{5}\left(\frac{m_s^2 + 2}{3}\right)^2 \left(\frac{m_p^2 - m_s^2}{4\pi m_s}\right)^2 \frac{4\pi M_0 \zeta e_s}{\rho N_A} \tag{21}$$

where $\zeta = 5.4$ is the number of monomeric units per statistical chain segment, $M_0 = 104\,\mathrm{g/mol}$ is the monomer molecular weight, and $e_s = 0.1$ is the optical shape factor for the segment (Kishbaugh, 1992; Kishbaugh and McHugh, 1993b). This contribution to $\Delta n'$ is also always positive.

Transient Rheo-optical Experiments

The steady-state rheo-optical data of Kishbaugh and McHugh (Kishbaugh, 1992; Kishbaugh and McHugh, 1993a) was obtained using a Couette flow cell subjected to the transient shear-rate profile depicted in Figure 2. In these experiments, the shear rate was ramped up from rest to the steady-state shear rate value of interest, $\dot{\gamma}_{ss}$, in a 2 s time interval. The shear rate was held constant for 5 s, and then it was ramped back down to rest in another 2 s interval. The 5 s steady-state interval was sufficient to allow the solutions to attain time-independent rheological and optical responses. These experiments were performed on polystyrene/decalin solutions made from monodisperse polymer samples of various molecular weights over a range of concentrations at 25°C.

Transient Data Fitting using the TCMM Model

The transient flow profiles for both the rheological and optical data reported by Kishbaugh and McHugh (Kishbaugh, 1992; Kishbaugh and McHugh, 1993a) will be analyzed in this section in terms of the TCMM model. In order to reproduce the results obtained from the transient experiments, the TCMM model must be applied to the transient shear profile of Figure 2. This is easiest to accomplish when working in terms of dimensionless quantities. Subsequently, the model predictions can be transformed back into dimensional quantities and compared with experimental data.

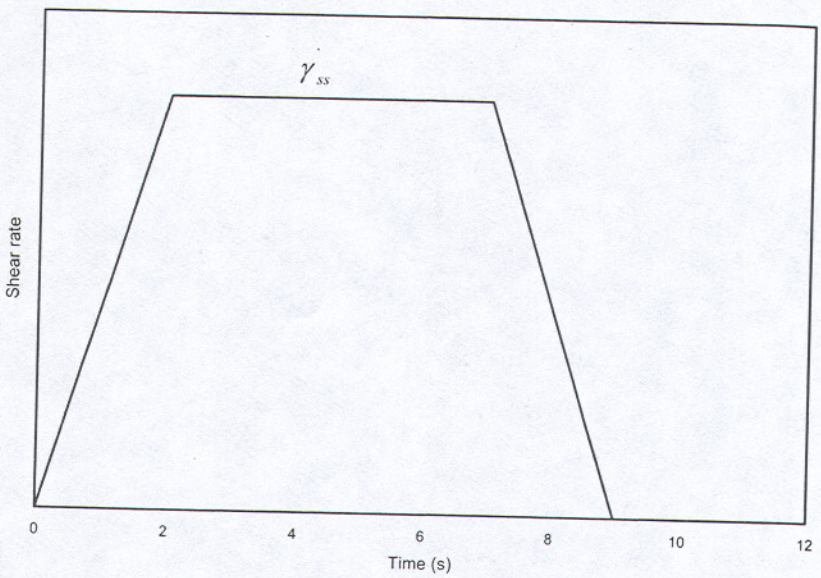

Figure 2. Trapezoidal velocity profile used for most of the rheo-optical measurements of Kishbaugh (1992) and Kishbaugh and McHugh (1993a).

The evolution equations, Equations (3) and (4), are made dimensionless by defining the dimensionless shear rate as $\tilde{\dot{\gamma}} \equiv \dot{\gamma}\sqrt{\lambda_1\lambda_2}$, the dimensionless mode tensors as $\tilde{c}^j_{\alpha\beta} \equiv K_j c^j_{\alpha\beta}/k_B T$, and dimensionless time as $\tilde{t} \equiv t/\sqrt{\lambda_1\lambda_2}$. Consequently, the spring constants, K_1 and K_2, drop out of the analysis, and one is left with only five parameters, λ_1, λ_2, n_1, n_2, and 0, that must be fit to the experimental data.

Fitting the model to experimental data was accomplished using two different methods. In Method 1, values for the five parameters listed above, as well as $\langle \mathbf{aa} \rangle_0$, can be taken directly from the previous study (Edwards et al., 2002; Jiang et al., 2003). In other words, the parameters are fitted using only *steady-state* viscosity versus shear rate data. Then the coupled, nonlinear, ordinary differential evolution equations, Equations (3) and (4), were solved using the fourth-order Runge-Kutta algorithm, in accordance with the transient shear flow profile of Figure 2. These equations are well conditioned, and hence stability issues were not relevant. This method is very stable and calculates time-dependent components of the two mode-conformation tensors to the desired degree of accuracy, in this case, to 12 significant figures. These components can then be converted into the requisite dimensional rheological and optical properties in a post-processing operation using Equations (5), (6), (7), and (17) and subsequently compared with available transient experimental data.

The second method, Method 2, was more complicated than the first. In this method, use is made of all available transient data taken for a given polymer molecular weight and concentration. Multiple transient dichroism profiles for various steady-state shear rates are fitted simultaneously using the Nelder and Mead downhill simplex method (Press et al., 1992) to find the best set of six parameters, λ_1, λ_2, n_1, n_2, 0, and $\langle \mathbf{aa} \rangle_0$, that give the smallest objective function. This objective function was defined as

$$f_{obj} = \left(\sum_{i=1}^{n_{set}} f_{obj}^{i} / n_T \right)^{1/2}, \quad f_{obj}^{i} = \sum_{j=1}^{n_d^i} w(j) \left(\frac{\Delta n''_{\text{expt}} - \Delta n''_{\text{model}}}{\Delta n''_{\text{expt}}} \right)^2 \tag{22}$$

where n_T is the total number of experimental data points from all transient dichroism profiles, n_{set} is the number of transient dichroism profiles, and n_d^i is the number of data points in the i-th data set. The weighting factor appearing in this expression was defined as $w(j) = 10$ when the experimental value of the dichroism was within 5% of its maximum value and $w(j) = 1$ otherwise.

The objective function thus represents an average of differences between the theoretical calculations and the experimental transient profiles for a given set of parameters. The Nelder and Mead algorithm searches through the parameter space trying to minimize the objective function, solving at each iteration the coupled evolution equations, Equations (3) and (4), and then calculating the dichroism to compare with the experimental transient dichroism profiles. (Dichroism profiles were used for the fitting, as opposed to stress or viscosity profiles, because none of the latter were presented in Kishbaugh (1992) and Kishbaugh and McHugh (1993a). After the objective function was minimized, the parameters corresponding to this value of objective function were used to compare the TCMM model with the transient experimental profiles.

Results

In all cases, data fitting was hindered by the limited transient data presented in the Kishbaugh and Mchugh publications (Kishbaugh 1992; Kishbaugh and Mchugh, 1993a). However, a sufficient amount of data could be gleaned from these sources to come to some significant conclusions, as described below.

Dichroism

Two sets of experimental transient dichroism curves are presented in Kishbaugh (1992) and Kishbaugh and McHugh (1993a). The first set is shown in Figure 3, along with TCMM model fits for the two data-fitting methods described in the preceding section. Experimental data in Figure 3 are for a solution of 6.8×10^6 g/mol polystyrene dissolved in decalin at a concentration of 0.30 g/dl. (In this and subsequent figures, only a sampling of results at specific values of the steady-state shear rate are shown; displayed results are typical.) The dashed curve corresponds to parameter values obtained using Method 1; these parameter values were obtained in Edwards et al., (2002) and are collected in Table I. Recall that these parameter values were obtained using steady-state viscosity versus shear rate curves (Edwards et al., 2002), such as represented symbolically in Figure 1. The solid curve corresponds to parameter values obtained via Method 2, which are also collected in Table I. Recall that these parameters were obtained by optimizing all available dichroism versus time curves simultaneously.

As evident, both sets of parameters describe well the qualitative features of the transient dichroism curves, but the latter set offers a fair amount of quantitative improvement, especially at lower shear rate values. The reason for this is apparent: the parameter values from Method 1 were obtained from the best model fit to steady-state viscosity versus shear rate data, whereas Method 2 optimized the

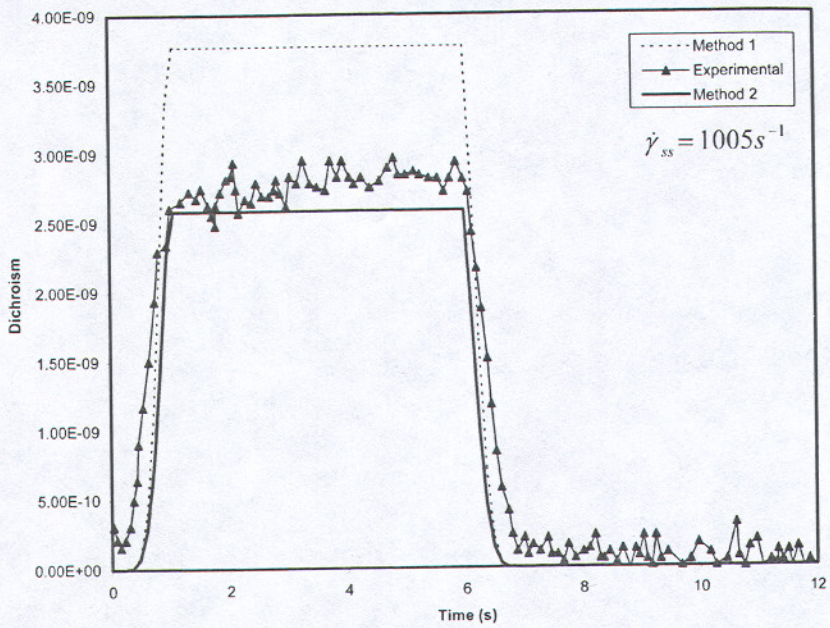

(a)

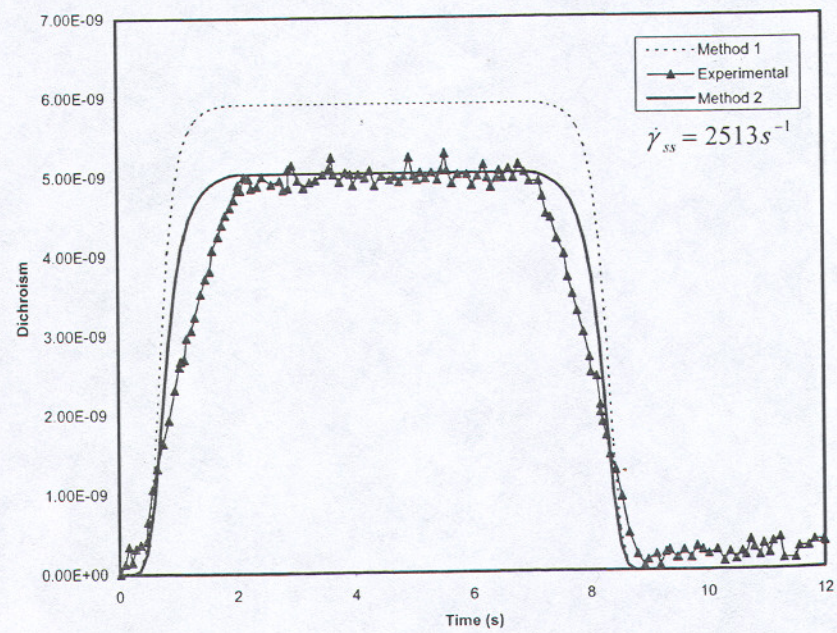

(b)

Figure 3. Transient dichroism for the solution with $c = 0.30$ g/dl at two steady-state shear rates.

Table I Parameter values for the 6.8×10^{6} g/mol Polystyrene/Decalin solution with $c = 0.30$ g/dl at 25°C

	λ_1(s)	λ_2(s)	n_1(mol/m^3)	n_2(mol/m^3)	θ	$\langle aa\rangle_0$(m^2)
Method 1	0.004333	0.013	1.0×10^{-3}	1.0×10^{-6}	0.10	4.20×10^{-16}
Method 2	0.001117	0.011	4.2×10^{-5}	4.1×10^{-7}	0.17	5.35×10^{-16}

Table II Parameter values for the 1.54×10^{6} g/mol Polystyrene/Decalin solution with $c = 0.79$ g/dl at 25°C

	λ_1(s)	λ_2(s)	n_1(mol/m^3)	n_2(mol/m^3)	θ	$\langle aa\rangle_0$(m^2)
Method 2	0.002769	0.0052	4.183×10^{-6}	4.181×10^{-6}	0.03	4.19×10^{-16}

Table III Parameter values for the 6.8×10^{6} g/mol Polystyrene/Decalin solution with $c = 0.10$ g/dl at 25°C

	λ_1(s)	λ_2(s)	n_1(mol/m^3)	n_2(mol/m^3)	θ	ω
Method 2	0.002258	0.0417	4.06×10^{-4}	9.22×10^{-7}	0.26	96.48

parameters to transient dichroism data, including those displayed in the figures. For this particular solution, no shear thickening was observed in the steady-state viscosity versus shear rate curve, nor did a maximum occur in the steady-state dichroism versus shear rate curve (Kishbaugh,1992; Kishbaugh and McHugh, 1993a; Edwards et al., 2002). At this concentration, the structure size increased with increasing shear rate, eventually reaching a limiting size at high shear rates (Edwards et al., 2002). According to the model and the experimental data, the size of the structures increases and the shape elongates monotonically to the steady-state structure size and shape upon start-up of shear, and decrease back to their quiescent values upon flow cessation.

Note that both theory and experiment coincide on another point: the dynamical response of the solution at any time is at a pseudo steady state. In other words, during start-up and cessation of flow, the instantaneous value of the shear rate determines the instantaneous values of all rheological and optical properties as if the flow field was at steady state with that particular value of the shear rate.

The orientation angles of the structures relative to the direction of flow are displayed in Figure 4 for one value of the steady-state shear rate. Here, only the TCMM model fit is displayed for the parameter values obtained via the more accurate Method 2. The model predicts well the transient qualitative features of the experimental data, including the initial rapid changes immediately after start-up and immediately before total flow cessation. Note that the experimental data contain much noise at very small and long times due to the method by which the orientation angle is calculated from the raw intensity data (Kishbaugh,1992; Kishbaugh and McHugh 1993a). This noise is not present in the TCMM model predictions, since

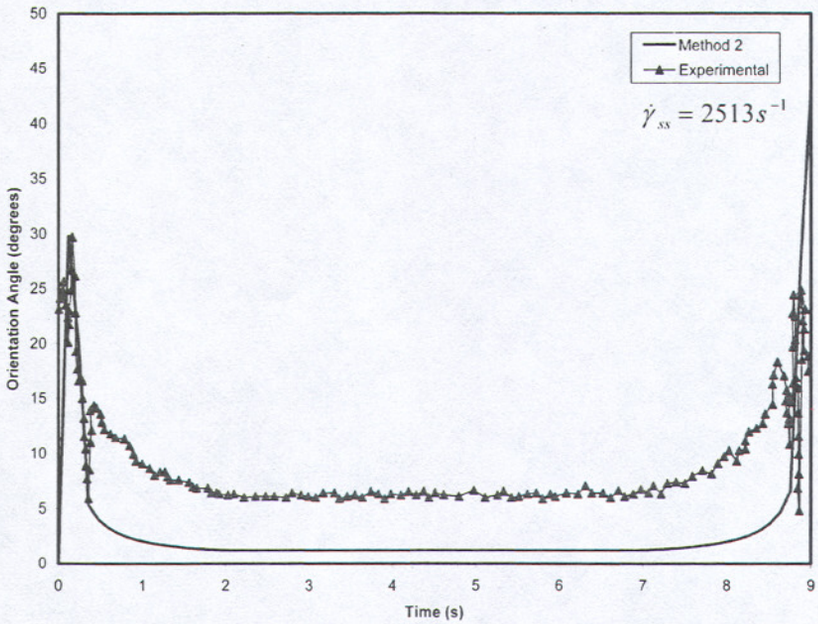

Figure 4. The orientation angle of the dichroism for the 6.8×10^6 g/mol polystyrene/decalin solution with $c = 0.30$ g/dl.

the computational algorithm is not subject to measurement error. At both values of the steady-state shear rate, the orientation angle drops quickly from its zero shear rate limit of 45° to a value fairly close to the direction of flow and then returns to 45° upon flow cessation.

The second set of dichroism data are much more interesting than the first in that this solution, a 1.54×10^6 g/mol polystyrene/decalin solution at a concentration of 0.79 g/dl, corresponds to a case in which the steady-state viscosity curve displays a minimum and the steady-state dichroism curve displays a maximum. Results of the TCMM model fit to the experimental data using the more accurate Method 2 are presented in Figure 5; parameter values are displayed in Table II. At the lowest value of the shear rate (not shown), the TCMM model captures the qualitative shape of the experimental curve, but the quantitative value is dramatically lower. This is consistent with the steady-state analysis of Edwards et al. (2002) and Jiang et al. (2003), wherein it was observed that the model is not quantitatively accurate at low shear rates. This problem is exacerbated by the greater degree of relative error in the experimentally measured value of the dichroism due to its small magnitude at low deformation rates. As the steady-state shear rate increases, the model becomes quantitatively accurate as well as qualitatively so. At the higher values of the steady-state shear rate, the curves display maxima upon start-up and cessation of flow. This occurs because the structures increase and then decrease in size and shape as the flow field approaches its steady state. At the highest values of the steady-state shear rate, the dichroism decreases to the point where it actually has a negative value, as indicated in Figure 5(c). At this point, the structures have become rather small and optically isotropic (i.e., spherical), and the dichroism is dominated by the inherent anisotropy of the individual chains remaining in solution (Edwards et al., 2002).

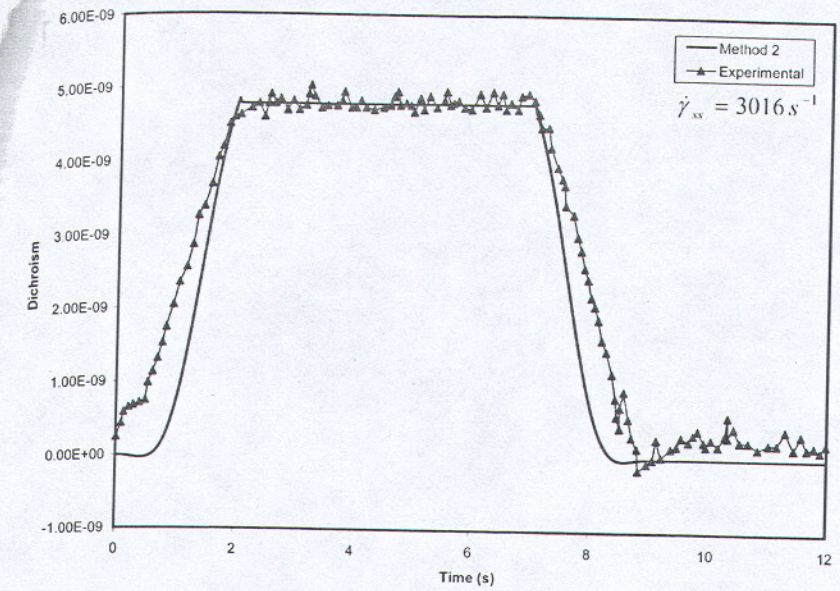

(a)

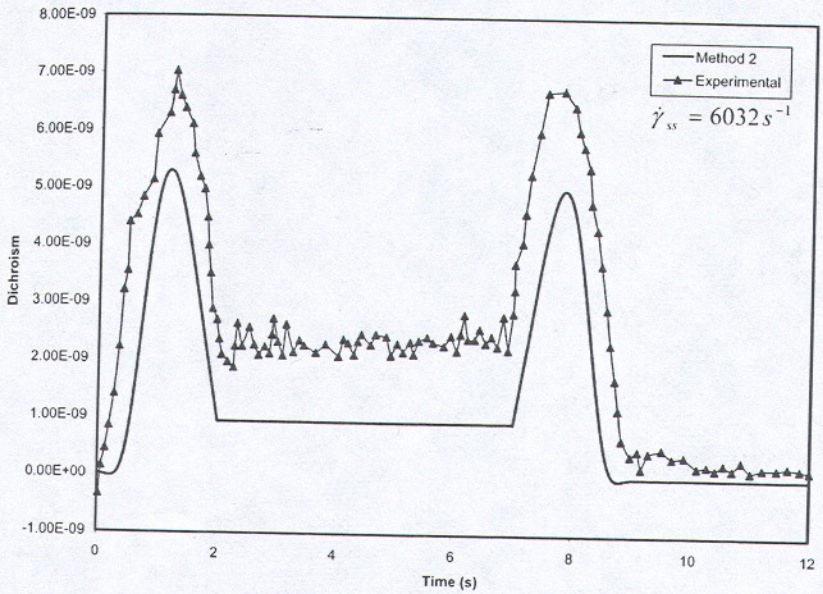

(b)

Figure 5. Transient dichroism for the 1.54×10^6 g/mol polystyrene/decalin solution with $c = 0.79$ g/dl at three steady-state shear rates.

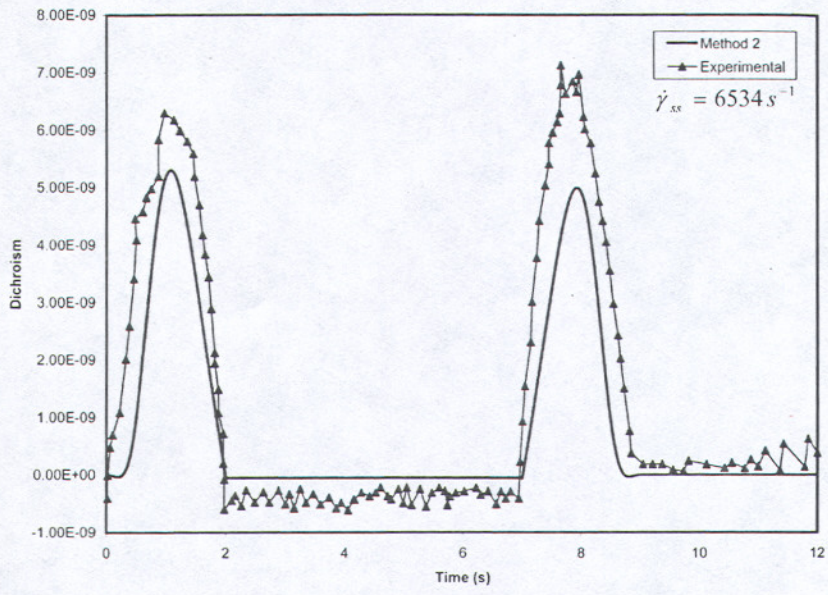

(c)

Figure 5. (Continued).

(Remember that polystyrene has a negative intrinsic optical anisotropy.) At flow cessation, the structures backtrack the path they took upon shear start-up until the solution returns to its quiescent condition.

The most interesting prediction of this analysis is obtained for the dichroic orientation angle for this solution at $\dot{\gamma}_{ss} = 7037s^{-1}$, as displayed in Figure 6. Recall that at this shear rate, the steady-state dichroism has a negative value, implying that the physical mechanism dominating the dichroic signal has switched from the structures to the individual polymer chains. Therefore, the model predicts that during flow start-up and flow cessation a discontinuity should appear in the orientation angle as the dominating mechanism switches from the structures to the chains. Hence the orientation angle switches discontinuously from that of the structures to that of the chains. (Although these data we not presented directly in Kishbaugh (1992) and Kishbaugh and McHugh (1993a), raw data for this case were given, so that the current authors were able to calculate the experimental curve.) It is evident that the experimental data display the same type of discontinuity at exactly the same times as the model predictions. This gives a strong validation of the notion initiated by Edwards et al., (2002) that the dichroism switches from a structure-controlled mechanism to an individual chain-controlled mechanism at very high shear rates.

Rheology

No transient rheological data are presented by Kishbaugh and McHugh for their rheo-optical experiments (Kishbaugh, 1992; Kishbaugh and McHugh, 1993a). However, they do state that for all cases, whether or not shear thickening was present, the shear stress curve almost exactly matched the trapezoidal shear profile of Figure 2. In Figure 7, we present plots of the shear stress versus time for the solutions of

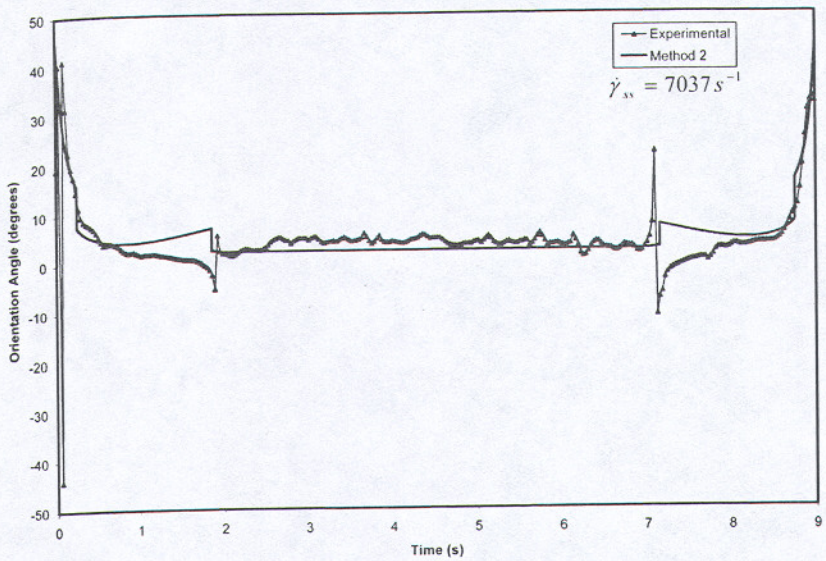

Figure 6. The orientation angle of the dichroism for the 1.54×10^6 g/mol polystyrene/decalin solution with $c = 0.79$ g/dl at $\dot{\gamma}_{ss} = 7037\ s^{-1}$.

Figure 4. It is evident that the observed stress profiles are consistent with the statement expressed above. Furthermore, the TCMM model also gives predictions for transient rheological properties that have not been measured experimentally. In Figures 8 and 9, we show predictions for both the first and second normal stress differences as functions of time at several values of the applied steady-state shear rate.

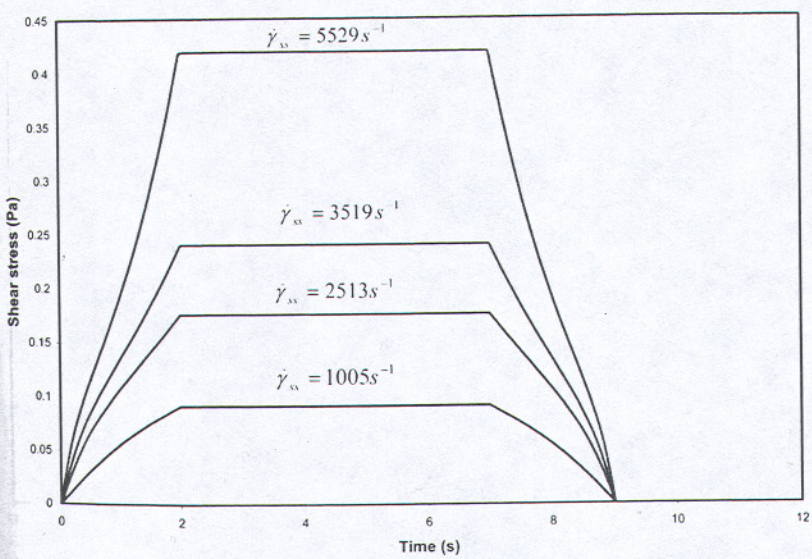

ıre 7. The shear stesses for the 6.8×10^6 g/mol polystyrene/decalin solution with 0.30 g/dl at four steady-state shear rates.

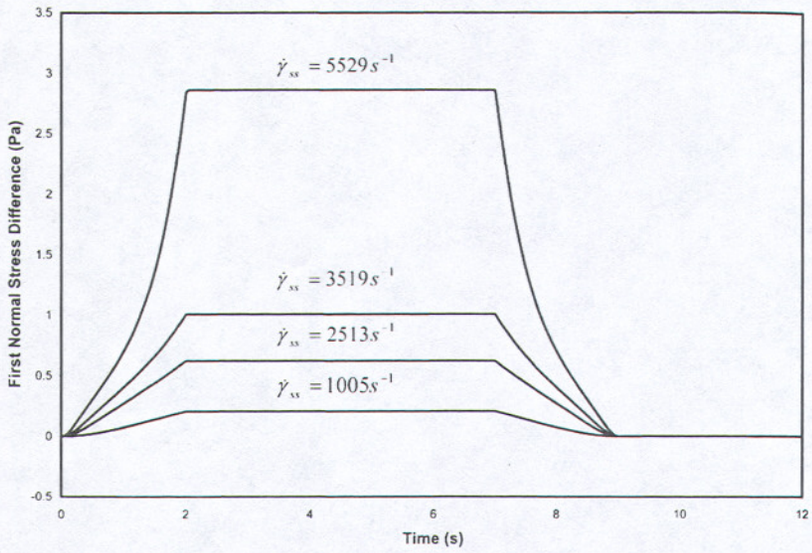

Figure 8. The first normal stress differences for the 6.8×10^6 g/mol polystyrene/decalin solution with $c = 0.30$ g/dl at four steady-state shear rates.

Birefringence

The TCMM model also describes reasonably well the linear birefringence as a function of time for shear-thickening dilute polymer solutions. In Figure 10, we plot the transient birefringence for several shear rates of a polystyrene/decalin solution from Kishbaugh (1992) and Kishbaugh and McHugh (1993a). For this set of

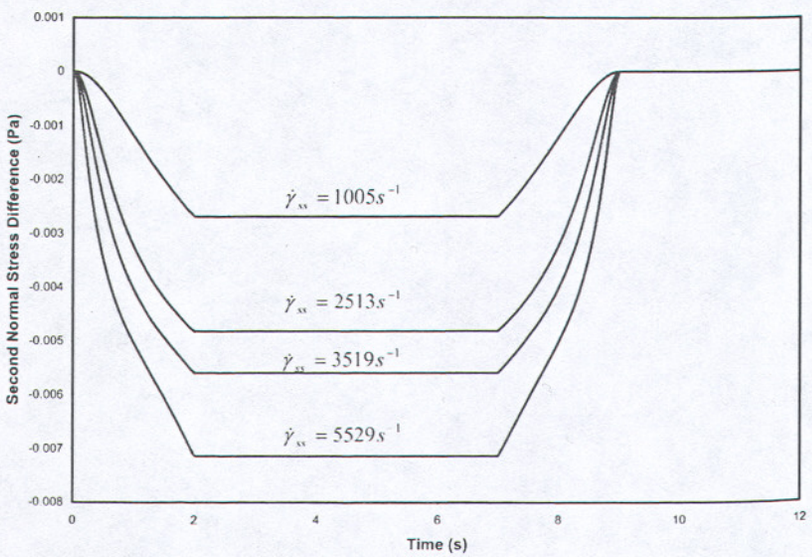

Figure 9. The second normal stress differences for the 6.8×10^6 g/mol polystyrene/decalin solution with $c = 0.30$ g/dl at four steady-state shear rates.

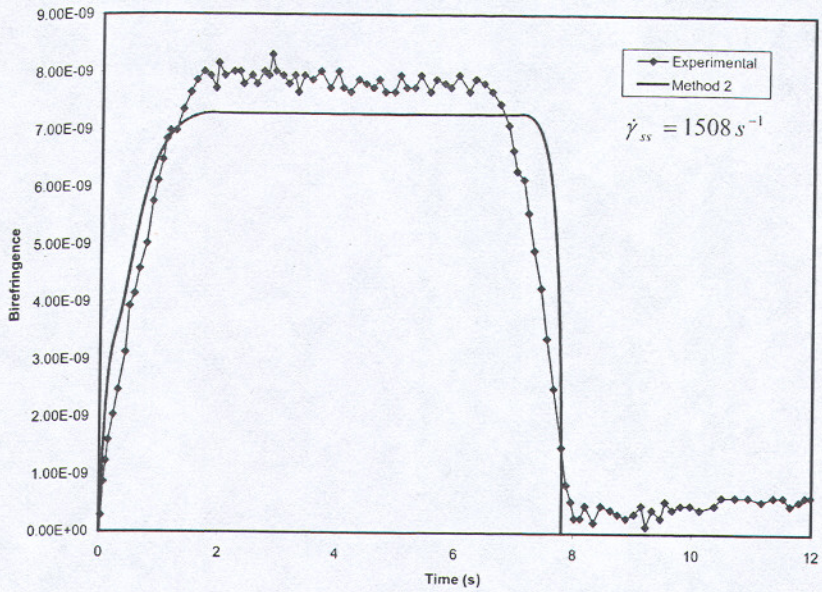

(a)

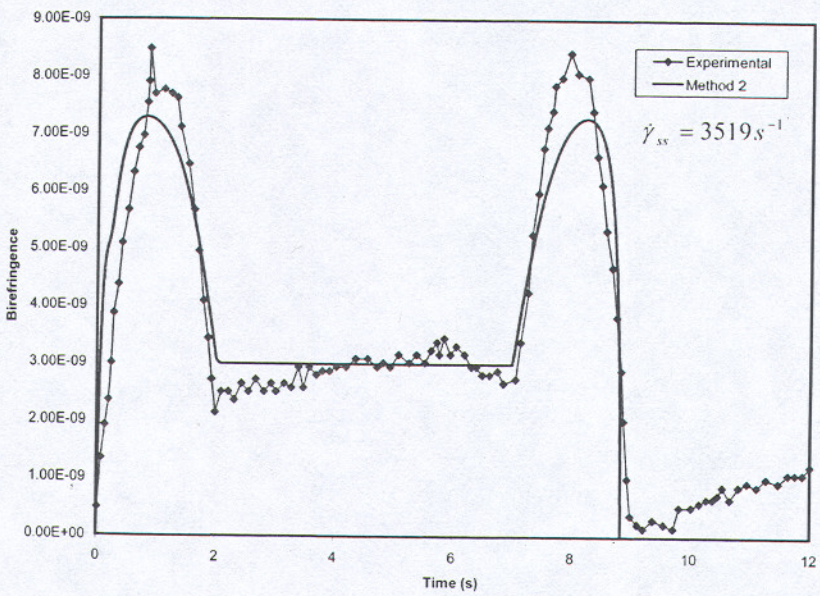

(b)

Figure 10. Transient birefringence for the 6.8×10^6 g/mol polystyrene/decalin solution with $c = 0.10$ g/dl at three steady-state shear rates.

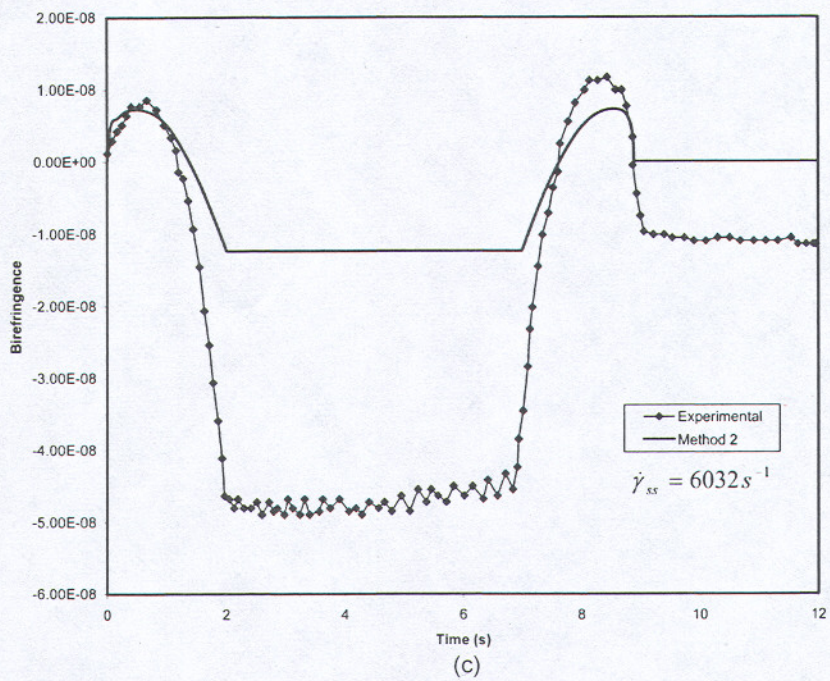

(c)

Figure 10. (Continued).

transient data, no dichroism data were available, so we fit the TCMM model to the birefringence data via Method 2, but using Equation (17) instead of the corresponding dichroism equation; parameter values are presented in Table III. At low shear rates, the birefringence is positive as the signal is dominated by form birefringence. As the steady-state shear rate increases, however, the birefringence turns negative as the intrinsic optical anisotropy of the stretched polystyrene chains takes over from the form birefringence. The fits to the experimental data are quite reasonable qualitatively, but differ quantitatively at the higher values of the steady-state shear rate. As noted in Edwards et al. (2002), the birefringence changed by several orders of magnitude with increasing shear rate, thus rendering a quantitative data fit quite difficult. The main problem with this fitting is that the birefringent signal must be positive at low shear rates and negative at high shear rates and the negative signals are of much larger magnitude than the positive ones. The issue then becomes whether one wants an accurate fit at low shear rates or at higher values. If one wants to fit higher values only, the parameter ω appearing in Equation (17) is not required.

Conclusions

In this article, we have focused on the transient analysis of the shear thickening in dilute polymer solutions. Using the TCMM model, we were able to reproduce the experimental results of the transient analysis with considerable accuracy. The analysis of the transient data is useful in the determination of the kinetics and reversibility of the structure formation process. Hence the TCMM model not only offers a

consistent explanation for the rheological and optical behavior associated with shear thickening (Edwards et al., 2002), but also provides valuable information about the kinetics of the phenomenon.

Some of the important conclusions of this analysis are as follows. The TCMM model was able to capture the reversibility and instantaneity of the structure formation as it showed the rapid increases and declines under the application of a trapezoidal shear rate profile. For the solutions that exhibit shear thickening, the transient dichroism changes sign for each steady-state shear rate above $\dot{\gamma}_m$. The orientation angle of the dichroism does not change sign, but we observe discontinuities in this quantity that correspond to the sign change in the dichroism signal from positive to negative. This gives a very good indication that the physical mechanism that dominates the dichroic signal has changed at this point in time, as suggested in Edwards et al. (2002).

References

Beris, A. N. and Edwards, B. J. (1994). *Thermodynamics of Flowing Systems*, Oxford University Press, New York.

Bird, R. B., Curtiss, C. F., Armstrong, R. C., and Hassager, O. (1987). *Dynamics of Polymeric Fluids*, 2nd ed., vol. 2, John Wiley, New York.

Copic, M. (1957). *J. Chem. Phys.*, **26**, 1382.

Edwards, B. J. and Beris, A. N. (1991a). *Ind. Eng. Chem. Res.*, **30**, 873.

Edwards, B. J. and Beris, A. N. (1991b). *J. Phys. A: Math. Gen.*, **24**, 2461.

Edwards, B. J., Beris, A. N., and Mavrantzas, V. G. (1996). *J. Rheol.*, **40**, 917.

Edwards, B. J., Keffer, D. J., and Reneau, C. W. (2002). *J. Appl. Polym. Sci*, **85**, 1714.

Grmela, M. (1988). *Phys. Lett. A*, **130**, 81.

Grmela, M. (1989). *J. Phys. A: Math. Gen.*, **22**, 4375.

Gurnee, E. F. (1954). *J. Appl. Phys.*, **25**, 1232.

Jiang, B., Keffer, D. J., Edwards, B. J., and Allred, A. N. (2003). *J. Appl. Polym. Sci.*, **90**, 2997.

Kishbaugh, A. J. (1992). The Rheo-Optics of Shear-Thickening and Structure Formation in Polymer Solutions, Ph.D. diss., University of Illinois.

Kishbaugh, A. J. and McHugh, A. J. (1993a). *Rheol. Acta*, **32**, 9.

Kishbaugh, A. J. and McHugh, A. J. (1993b). *Rheol. Acta*, **32**,115.

Kuhn, W. and Grün, F. (1942). *Kolloid-Z.*, **101**, 248.

Layec-Raphalen, M. and Wolff, C. (1976). *J. Non-Newtonian Fluid Mech.*, **1**, 159.

Press, W. H., Vettuling, W. T., Tevkolsky, S. A., and Flannery, B. P. (1992). *Numerical Recipes in Fortran 77*, Cambridge University Press, Cambridge.

Tsvetkov, V. N. (1964). *Sov. Phys. Usp.*, **6**, 639.

Vrahopoulou, E. P. and McHugh, A. J. (1987). *J. Non-Newtonian Fluid Mech.*, **25**, 157.